Chemical Science

ROYAL SOCIETY OF CHEMISTRY

EDGE ARTICLE

View Article Online
View Journal | View Issue

Check for updates

Cite this: *Chem. Sci.*, 2025, **16**, 6114

All publication charges for this article have been paid for by the Royal Society of Chemistry

Received 23rd December 2024
Accepted 6th March 2025

DOI: 10.1039/d4sc08647c

rsc.li/chemical-science

Open Access Article. Published on 07 March 2025. Downloaded on 2/15/2026 10:58:22 PM. This article is licensed under a Creative Commons Attribution-NonCommercial 3.0 Unported Licence.

Configurational control of low-symmetry heteroleptic metal–organic cages with asymmetric ligands†

Hao Yu, Ziteng Guo, Jie Tang, Ningxu Han, Junjuan Shi, Meng Li, Houyu Zhang and Ming Wang *

Low-symmetry metal–organic cages (MOCs) can better mimic the structure of biological enzymes compared to high-symmetry MOCs, due to their unique internal cavities that resemble the specialized and irregular active sites of enzymes. In this study, two low-symmetry heteroleptic MOCs with six Pd(II) centers, $Pd_6L^A{}_6L^B{}_6$ and $Pd_6L^B{}_6L^C{}_6$, were successfully constructed by combining two strategies: asymmetric ligand assembly and multi-ligand co-assembly. Crystallographic characterization and analysis revealed that $Pd_6L^A{}_6L^B{}_6$ is a mixture of potentially 16 isomers. Introducing a methyl group at the *ortho* position of the coordination site of ligand L^C induced steric hindrance, driving $Pd_6L^B{}_6L^C{}_6$ to undergo a structural transformation and selectively assemble into a single dominant configuration from 13 potential isomers. This work not only demonstrates the immense potential of integrating asymmetric ligand assembly with multi-ligand co-assembly strategies but also highlights the critical role of steric effects in guiding assembly pathways and achieving precise configurational control in low-symmetry MOCs.

Introduction

Metal–organic cages (MOCs) with discrete three-dimensional structures are formed through the self-assembly of diverse organic ligands and metal ions.[1–9] MOCs have garnered significant attention from researchers, due to their highly adjustable structures and versatile functionalities, such as molecular recognition, separation, and catalysis.[10–18] Consequently, they are frequently employed to emulate the functions of biological enzymes. However, most reported MOCs are constructed using symmetric ligands and metal ions, leading to highly symmetric structures. While some symmetric MOCs can exhibit high selectivity and catalytic efficiency for specific substrates due to their well-defined spatial and electronic environments,[19–21] they often lack the unique and irregular internal cavities found in natural enzymes. These cavities are crucial for achieving broader substrate specificity and distinctive catalytic functions. Therefore, developing low-symmetry MOCs is essential for advancing biomimetic applications.

In general, there are two approaches for constructing low-symmetry MOCs: the first approach involves reducing the symmetry of ligands, utilizing a single type of asymmetric ligands to construct low-symmetry MOCs.[22–29] A representative example is Lewis's ingenious use of asymmetric ligands to assemble various low-symmetry Pd_2L_4 molecular cages.[30,31] The second approach is employing co-assembly of two or more types of symmetric ligands to build low-symmetry MOCs.[32–39] The most notable example is Clever's recent report on the co-assembly of four different ligands, resulting in the formation of a heteroleptic cage, Pd_2ABCD.[40] Combining these two approaches presents a valuable opportunity to develop more complex low-symmetry MOCs. However, each strategy poses specific challenges in achieving precise low-symmetry MOCs. In the case of self-assembly based on asymmetric ligands, the main challenge lies in preventing the formation of multiple isomers with similar stability. For heteroleptic systems, the difficulty is to avoid the formation of homoleptic complexes or statistical mixtures. Consequently, integrating these two approaches will inevitably complicate the assembly process. To date, as far as we know, only five reported examples have successfully integrated these approaches using different strategies. Lewis employed coordination sphere engineering,[41] Preston utilized an auxiliary pairing strategy,[42] Chand applied the geometric complementarity principle,[43] and Bloch, Fallon,[44] and Pilgrim[45] used different isomeric structures with asymmetry to construct distinct dinuclear Pd(II) low-symmetry MOCs. These achievements highlight the potential of combining these

State Key Laboratory of Supramolecular Structure and Materials, College of Chemistry, Jilin University, Changchun 130012, China. E-mail: mingwang358@jlu.edu.cn

† Electronic supplementary information (ESI) available: Synthetic details and characterizations of ligands and complexes including NMR, ESI-MS, X-ray crystallographic data and DFT calculations. Moreover, it also contains the number of theoretically possible isomers of $Pd_{12}L^A{}_{24}$, $Pd_6L^A{}_6L^B{}_6$-**a** and $Pd_6L^A{}_6L^B{}_6$-**b**. CCDC 2387801, 2387551 and 2387553. For ESI and crystallographic data in CIF or other electronic format see DOI: https://doi.org/10.1039/d4sc08647c

© 2025 The Author(s). Published by the Royal Society of Chemistry

Open Access Article. Published on 07 March 2025. Downloaded on 2/15/2026 10:58:22 PM. This article is licensed under a Creative Commons Attribution-NonCommercial 3.0 Unported Licence.

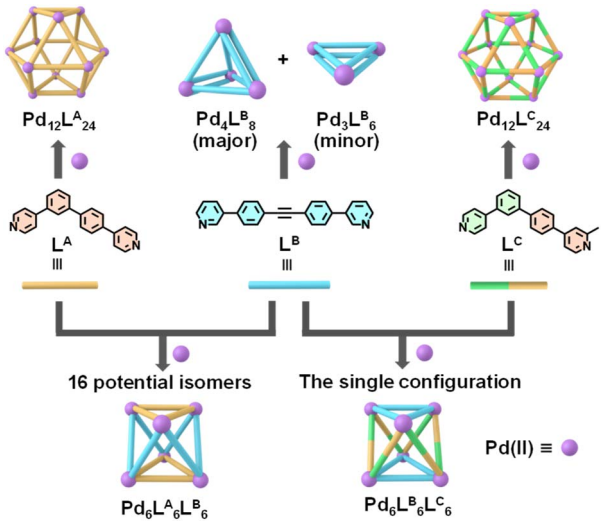

Fig. 1 Metal–organic cages assembled from L^A, L^B and L^C with Pd(II).

methods. However, further exploration of this integration to create low-symmetry heteroleptic MOCs with higher nuclearity and achieve configurational control remains a significant challenge.

In this study, we designed and synthesized asymmetric ligands $\mathbf{L^A}$ and $\mathbf{L^C}$, along with symmetric ligand $\mathbf{L^B}$ (Fig. 1). When individually used with Pd(II) for assembly, all three ligands can form discrete structures. Co-assembly of $\mathbf{L^A}$, $\mathbf{L^B}$, and Pd(II) resulted in the formation of hexanuclear low-symmetry heteroleptic MOCs, $\mathbf{Pd_6L^A{}_6L^B{}_6}$. Crystallographic characterization and analysis revealed that $\mathbf{Pd_6L^A{}_6L^B{}_6}$ is a mixture of potentially 16 isomers. To achieve precise configurational control in the heteroleptic cage assembly, a methyl group was introduced at the *ortho* position of one coordination site on $\mathbf{L^C}$, based on the $\mathbf{L^A}$, to induce steric hindrance during the assembly process. This specific position was chosen to maximize control over the assembly direction and reduce the number of possible isomers. Experimental results showed that the introduction of methyl groups did not alter the overall composition of either the homoleptic or heteroleptic cages, but it positively influenced configurational control. Co-assembly of $\mathbf{L^C}$ with $\mathbf{L^B}$ and Pd(II) effectively controlled the assembly process, directing the formation of a single dominant configuration of the low-symmetry heteroleptic MOCs, $\mathbf{Pd_6L^B{}_6L^C{}_6}$, from 13 possible isomers. This study highlights the successful integration of asymmetric ligand assembly with heteroleptic co-assembly for constructing high-nuclearity, low-symmetry heteroleptic MOCs and demonstrates the effectiveness of using steric hindrance to achieve precise configurational control.

Results and discussion

Guided by the principle of geometric complementarity, we designed $\mathbf{L^A}$ and $\mathbf{L^B}$ to coordinate with "naked" Pd(II) ions, enabling the formation of heteroleptic cages. To explore the role of steric effects, we further designed the other asymmetric ligand $\mathbf{L^C}$ by introducing a methyl group at the *ortho* position of the nitrogen atom and studied its impact on the assembly of heteroleptic cages. The ligands $\mathbf{L^A}$, $\mathbf{L^B}$, and $\mathbf{L^C}$ were synthesized through the efficient Suzuki and Sonogashira coupling reaction, and the detailed synthetic routes and characterizations were shown in the ESI (Schemes S1–S3 and Fig. S1–S5, S10–S14, S20–S24, and S42–S44).† We began by examining the assembly of ligands $\mathbf{L^A}$ and $\mathbf{L^B}$ with Pd(II) individually. To investigate this, $\mathbf{L^A}$ was assembled with $Pd(CH_3CN)_4(BF_4)_2$ in DMSO-d_6 at a 2 : 1 molar ratio at 70 °C overnight to form the assembly based on $\mathbf{L^A}$. In the ^{1}H NMR spectrum, five broad peaks were observed, indicating the formation of a large complex with slow tumbling on the NMR timescale (Fig. 2a). Subsequently, ESI-MS was used to confirm the molecular composition of the $\mathbf{L^A}$ assembly, revealing a series of peaks with successive charge states, corresponding to the loss of varying numbers of BF_4^- counterions. The observed charge fragments include m/z = 1257.76 for $[\mathbf{Pd_{12}L^A{}_{24}}(BF_4)_{16}]^{8+}$, 1108.32 for $[\mathbf{Pd_{12}L^A{}_{24}}(BF_4)_{15}]^{9+}$, 988.90 for $[\mathbf{Pd_{12}L^A{}_{24}}(BF_4)_{14}]^{10+}$, 891.01 for $[\mathbf{Pd_{12}L^A{}_{24}}(BF_4)_{13}]^{11+}$, and 809.57 for $[\mathbf{Pd_{12}L^A{}_{24}}(BF_4)_{12}]^{12+}$ (Fig. 2b, S45 and S46†). By calculating the molecular ion peaks, the molecular weight of the $\mathbf{L^A}$ assembly was determined to be 10,753.9 Da, corresponding to 24 $\mathbf{L^A}$, 12 Pd(II) ions, and 24 BF_4^-. Although these characterizations confirmed that the asymmetric ligand $\mathbf{L^A}$ and Pd(II) could form a $\mathbf{Pd_{12}L^A{}_{24}}$ assembly, the exact configuration of $\mathbf{Pd_{12}L^A{}_{24}}$ remained unclear. To resolve this, we aim to use single-crystal characterization to determine the exact structure of the $\mathbf{Pd_{12}L^A{}_{24}}$ assembly. By allowing ethyl acetate vapor to diffuse into a DMF solution of $\mathbf{(Pd_{12}L^A{}_{24})(OTf)_{24}}$ over approximately two months, we obtained crystals suitable for testing diffraction experiments. The single-crystal data was collected by using synchrotron radiation (Table S1, Fig. S56 and S57†) and revealed that in $\mathbf{Pd_{12}L^A{}_{24}}$, each asymmetric ligand exhibits disorder and can adopt two possible orientations (shown as yellow and gray ligands in Fig. 2c). This disorder results from the absence of energetic preference for any specific isomer within the assembly, leading to multiple isomers coexisting in solution and crystallizing as a statistical mixture.[46] Using Pólya's theorem, we calculated the total number of potential isomers to be 700 688 (Fig. S62†), which aligns with results reported in the literature.[23,47] The assembly based on $\mathbf{L^B}$ was obtained by mixing $\mathbf{L^B}$ and $Pd(CH_3CN)_4(BF_4)_2$ in DMF-d_7 at a stoichiometric ratio of 2 : 1, and then heated at 70 °C overnight. The obtained assembly showed two sets of proton peaks (Fig. 2d) with an approximate ratio of 4 : 1, indicating the presence of a dynamic equilibrium mixture of two thermodynamically similar assemblies in solution. This observation was further corroborated by DOSY measurements, which clearly resolved two distinct diffusion bands, confirming the presence of two discrete species in solution (Fig. S18†). The primary assembly (black) displayed two distinct chemical environments for its ligands, while the secondary assembly (red) showed only one. ESI-MS characterization identified that the assembly product for $\mathbf{L^B}$ is a mixture of the octameric $\mathbf{Pd_4L^B{}_8}$ and the hexameric $\mathbf{Pd_3L^B{}_6}$, with the former being the major product (Fig. 2e). By integrating NMR, ESI-MS, and the earlier research report,[48] we proposed structural models for both $\mathbf{Pd_4L^B{}_8}$ and $\mathbf{Pd_3L^B{}_6}$ (Fig. 2f and g).

Open Access Article. Published on 07 March 2025. Downloaded on 2/15/2026 10:58:22 PM.
This article is licensed under a Creative Commons Attribution-NonCommercial 3.0 Unported Licence.

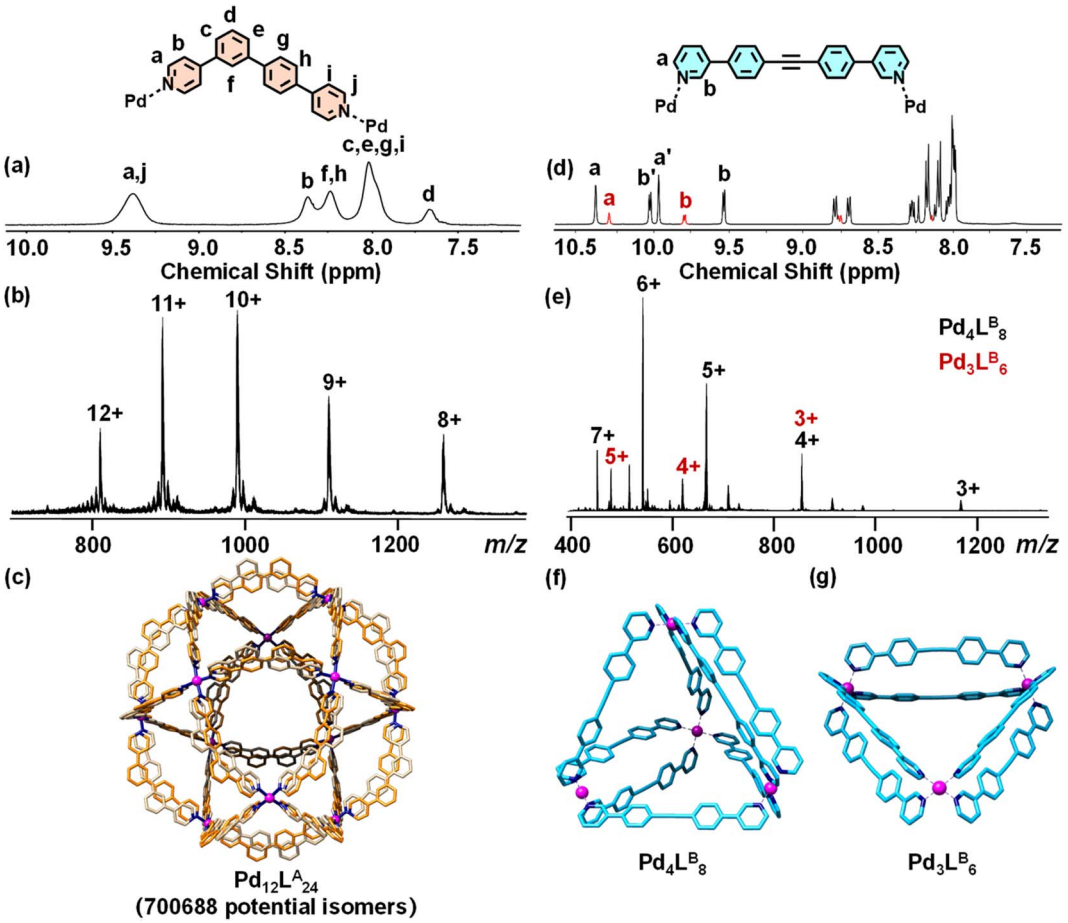

Fig. 2 ^{1}H NMR spectra (500 MHz, 300 K) of (a) $Pd_{12}L^A_{24}$, (d) $Pd_4L^B_8$ and $Pd_3L^B_6$; ESI-MS spectra of (b) $Pd_{12}L^A_{24}$, (e) $Pd_4L^B_8$ and $Pd_3L^B_6$; (c) the single-crystal structure of $Pd_{12}L^A_{24}$; structural simulations of (f) $Pd_4L^B_8$ and (g) $Pd_3L^B_6$ (hydrogen atoms are omitted for clarity).

After characterizing the assemblies of $\mathbf{L^A}$ and $\mathbf{L^B}$ individually, we explored their co-assembly with Pd(II). A 1 : 1 : 1 molar ratio of $\mathbf{L^A}$, $\mathbf{L^B}$, and $Pd(CH_3CN)_4(BF_4)_2$ was dissolved in DMF-d_7, and the mixture was reacted at 70 °C overnight. The ^{1}H NMR spectrum of the co-assembly exhibited distinct chemical shifts compared to the individual assemblies of $\mathbf{L^A}$ and $\mathbf{L^B}$, indicating the formation of new structure (Fig. S29 and S37†). However, some weaker peaks indicating side products were also observed during the assembly process, and multiple attempts to eliminate these signals were unsuccessful. ESI-MS displayed a sequence of peaks with successive charge states, corresponding to the following *m*/*z* values: 1294.72 for $[\mathbf{Pd_6L^A_6L^B_6}(BF_4)_8]^{4+}$, 1018.61 for $[\mathbf{Pd_6L^A_6L^B_6}(BF_4)_7]^{5+}$, 834.36 for $[\mathbf{Pd_6L^A_6L^B_6}(BF_4)_6]^{6+}$, 702.82 for $[\mathbf{Pd_6L^A_6L^B_6}(BF_4)_5]^{7+}$, 604.21 for $[\mathbf{Pd_6L^A_6L^B_6}(BF_4)_4]^{8+}$, and 527.53 for $[\mathbf{Pd_6L^A_6L^B_6}(BF_4)_3]^{9+}$ (Fig. 3b, S52 and S53†). Calculation of the molecular ion peaks determined a molecular weight of 5521.03 Da for the co-assembly, consistent with a structure composed of six $\mathbf{L^A}$, six $\mathbf{L^B}$, six Pd(II) ions, and twelve BF_4^- ions. This confirms the successful construction of a mixed-ligand metal–organic cage, $\mathbf{Pd_6L^A_6L^B_6}$, based on asymmetric ligands. Based on our analysis and simulations, we propose that the $\mathbf{Pd_6L^A_6L^B_6}$ cage may exist in two different structural types, namely $\mathbf{Pd_6L^A_6L^B_6}$-**a** and $\mathbf{Pd_6L^A_6L^B_6}$-**b** (Fig. 3a). This is primarily attributed to the specific molecular angles, coordination sites, and ligand lengths of the two ligands, which promote geometric complementarity in coordination with Pd(II) ions. This complementarity directs the assembly process toward the formation of these two possible structures while preventing the formation of other isomers. Due to the disorder of the asymmetric ligand $\mathbf{L^A}$, both $\mathbf{Pd_6L^A_6L^B_6}$-**a** and $\mathbf{Pd_6L^A_6L^B_6}$-**b** have multiple potential isomers. Using an enumeration method, we identified 13 possible isomers for $\mathbf{Pd_6L^A_6L^B_6}$-**a** (Fig. S64†) and 16 possible isomers for $\mathbf{Pd_6L^A_6L^B_6}$-**b** (Fig. S63†). To further determine the configuration of the heteroleptic cage, we obtained the single crystal by slow diffusion of ethyl acetate into a DMF solution of $\mathbf{Pd_6L^A_6L^B_6}$ about three weeks (Table S2, Fig. S58 and S59†). As seen in Fig. 3c, the resulting crystal structure corresponds to the structural type $\mathbf{Pd_6L^A_6L^B_6}$-**b**. In this structure, the asymmetric ligands $\mathbf{L^A}$ are located on opposite sides of the molecular cage, while the ligands $\mathbf{L^B}$ are positioned in the center, connecting with each other. Additionally, each $\mathbf{L^A}$ in $\mathbf{Pd_6L^A_6L^B_6}$ exhibits disorder, allowing two possible orientations, similar to the arrangement of ligands in the $\mathbf{Pd_{12}L^A_{24}}$ (shown as yellow and gray ligands in Fig. 3c). This suggests that $\mathbf{Pd_6L^A_6L^B_6}$ can exist in solution as a statistical mixture of up to 16 isomers, resulting in the crystallization of a variety of structures.

© 2025 The Author(s). Published by the Royal Society of Chemistry

Open Access Article. Published on 07 March 2025. Downloaded on 2/15/2026 10:58:22 PM. This article is licensed under a Creative Commons Attribution-NonCommercial 3.0 Unported Licence.

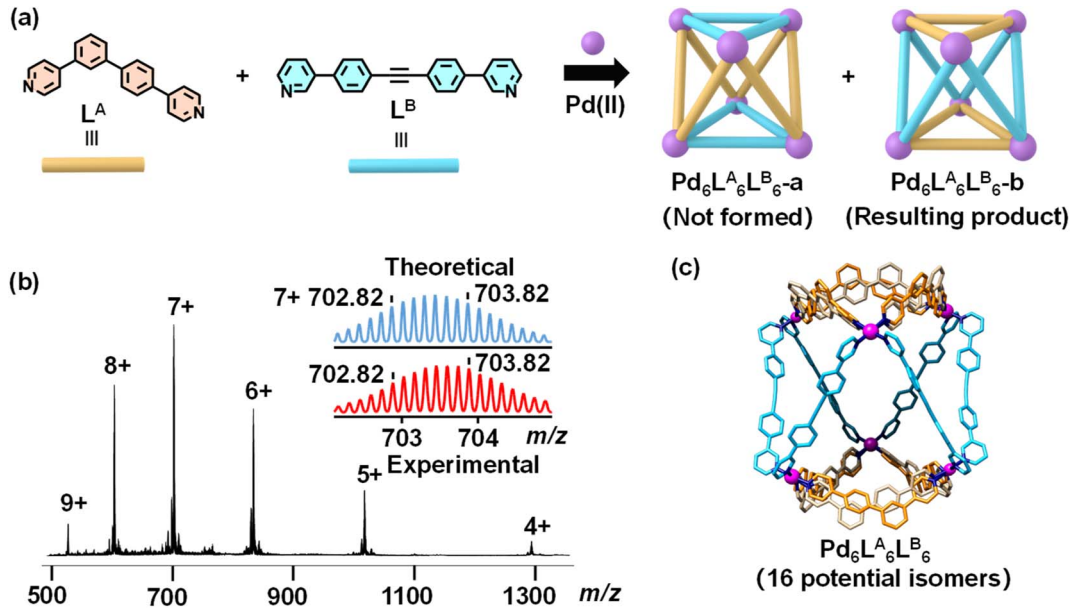

Fig. 3 (a) Two possible structural types of $Pd_6L^A{}_6L^B{}_6$; (b) ESI-MS spectrum of $Pd_6L^A{}_6L^B{}_6$; (c) the crystal structure of $Pd_6L^A{}_6L^B{}_6$ (hydrogen atoms are omitted for clarity).

Employing steric group modifications on ligands to enhance spatial constraints during assembly serves as an effective strategy for controlling configuration. However, current research primarily targets simpler M_2L_4 molecular cages with fewer components.[30,49–51] We wanted to investigate whether this strategy could be used to control the configuration of more complex heteroleptic cages. To achieve this, we utilized $\mathbf{L^C}$, featuring methyl group modifications on a single side of the pyridine as steric hindrance, in conjunction with $\mathbf{L^B}$ and Pd(II) for co-assembly. The assembly method was the same as that used for $\mathbf{Pd_6L^A{}_6L^B{}_6}$. The ^{1}H NMR spectrum of the co-assembly showed significant chemical shifts relative to the individual assemblies of $\mathbf{L^B}$ and $\mathbf{L^C}$, indicating the formation of heteroleptic product (Fig. S33 and S38†). However, we also detected smaller proton peaks corresponding to side products. Despite multiple experimental attempts, we couldn't eliminate or reduce these signals. ESI-MS characterization confirmed the co-assembly as a heteroleptic metal–organic cage with six $\mathbf{L^B}$ and six $\mathbf{L^C}$ (Fig. 4b). By slowly evaporating ethyl acetate into a DMF solution of $\mathbf{Pd_6L^B{}_6L^C{}_6}$, the single crystals suitable for testing were successfully obtained (Table S3, Fig. S60 and S61†). The configuration of $\mathbf{Pd_6L^B{}_6L^C{}_6}$ may also have two structural types, namely $\mathbf{Pd_6L^B{}_6L^C{}_6}$-**a** and $\mathbf{Pd_6L^B{}_6L^C{}_6}$-**b** (Fig. 4a). Similarly, they also have 13 and 16 potential isomers, respectively. From Fig. 4c, it is evident that the observed crystal structure aligns with our prediction of the structural type $\mathbf{Pd_6L^B{}_6L^C{}_6}$-**a**, where ligand $\mathbf{L^B}$ forms the top and bottom of the molecular cage, while the asymmetric ligand $\mathbf{L^C}$ is located in the middle and interconnected. It is particularly noteworthy that, unlike the disordered distribution of asymmetric ligands in $\mathbf{Pd_6L^A{}_6L^B{}_6}$, asymmetric ligand $\mathbf{L^C}$ in $\mathbf{Pd_6L^B{}_6L^C{}_6}$ exhibits a regular *cis* arrangement in the molecular cage due to the presence of sterically hindered methyl groups. We propose that the introduction of this steric hindrance effectively regulates intermolecular interactions and spatial organization, resulting in a more orderly assembly process and reducing isomer formation. Within each Pd(II) center of the $\mathbf{Pd_6L^B{}_6L^C{}_6}$-**a** cage, there are three unmodified pyridine groups and one methyl-modified pyridine group. This arrangement arises because the presence of two or more methyl groups on the same Pd(II) center would lead to significant steric hindrance. Consequently, the most stable configuration naturally avoids such steric clashes, and this arrangement represents the optimal binding mode achieved through coordination-driven self-assembly.

We performed Density Functional Theory (DFT) calculations on $\mathbf{Pd_6L^B{}_6L^C{}_6}$-**a** and $\mathbf{Pd_6L^B{}_6L^C{}_6}$-**b**. To align with experimental conditions, we considered solvent effects using a linearized Poisson–Boltzmann solvation model to represent the impact of DMF. The results indicated that $\mathbf{Pd_6L^B{}_6L^C{}_6}$-**a** had lower energy, with an energy difference of 7.39 kJ mol^{-1} compared to $\mathbf{Pd_6L^B{}_6L^C{}_6}$-**b** (Fig. 4d). This suggests that $\mathbf{Pd_6L^B{}_6L^C{}_6}$-**a** is energetically favored, which aligns well with the crystal characterization result. We hypothesize that this is due to the structure of $\mathbf{Pd_6L^B{}_6L^C{}_6}$-**a** is capable of more effectively alleviating the steric hindrance induced by the methyl group, in contrast to $\mathbf{Pd_6L^B{}_6L^C{}_6}$-**b**. By integrating NMR, ESI-MS, X-ray crystallography and DFT calculations, we observed that compared with $\mathbf{Pd_6L^A{}_6L^B{}_6}$, $\mathbf{Pd_6L^B{}_6L^C{}_6}$ not only underwent a structural transformation but also selectively assembled into a single dominant configuration from 13 possible isomers. This indicates that the strategy of introducing steric groups on asymmetric ligands has successfully achieved configurational control in low-symmetry heteroleptic MOCs. Additionally, using NMR and ESI-MS, we confirmed that the assembly product of $\mathbf{L^C}$ and Pd(II) is $\mathbf{Pd_{12}L^C{}_{24}}$ (Fig. S25 and S45†). Although we didn't obtain the crystal structure to determine the precise arrangement of $\mathbf{Pd_{12}L^C{}_{24}}$, variable-temperature NMR and

Open Access Article. Published on 07 March 2025. Downloaded on 2/15/2026 10:58:22 PM. This article is licensed under a Creative Commons Attribution-NonCommercial 3.0 Unported Licence.

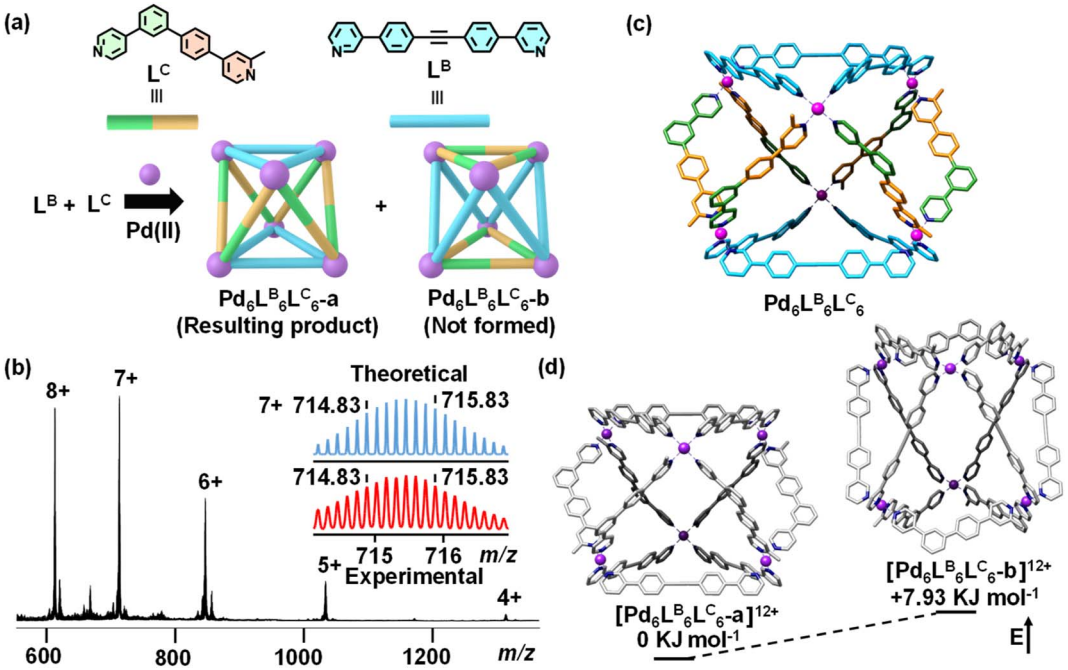

Fig. 4 (a) Two possible structural types of $Pd_6L^B{}_6L^C{}_6$; (b) ESI-MS spectrum of $Pd_6L^B{}_6L^C{}_6$; (c) the crystal structure of $Pd_6L^B{}_6L^C{}_6$; (d) calculated structures and relative energies of $[Pd_6L^B{}_6L^C{}_6\text{-a}]^{12+}$ and $[Pd_6L^B{}_6L^C{}_6\text{-b}]^{12+}$ (hydrogen atoms are omitted for clarity).

DFT calculations suggest that it might adopt a ***trans*-$Pd_{12}L^C{}_{24}$** configuration (Fig. S39, S65 and S66†), indicating that steric strategy might also be useful for tuning the structure of more complex large molecular cages with more components.

Conclusions

In summary, by combining asymmetric ligand assembly with heteroleptic co-assembly, we successfully synthesized six-nuclear, low-symmetry heteroleptic MOCs, $Pd_6L^A{}_6L^B{}_6$ and $Pd_6L^B{}_6L^C{}_6$. Crystallographic analysis revealed that $Pd_6L^A{}_6L^B{}_6$ has 16 possible isomers. In contrast, the methyl-modified ligand L^C introduced steric hindrance during assembly, leading to a structural transformation and configuration control in $Pd_6L^B{}_6L^C{}_6$. This study highlights the potential of integrating asymmetric ligand assembly with mixed-ligand co-assembly to construct complex, high-nuclearity, low-symmetry molecular architectures. Furthermore, it underscores the crucial role of steric effects in controlling the configuration of MOCs.

Data availability

The data supporting this article have been included as part of the ESI.†

Author contributions

In this work, M. W. and H. Y. conceived and designed the experiments. H. Y., Z. G and J. T. completed the synthesis. H. Y. grew the crystal and collected X-ray data of the crystals. H. Z. performed the DFT calculations. H. Y. and Z. G. conducted NMR, MS characterization. M. W., H. Y., N. H, J. S. and M. L. analyzed the data and wrote the manuscript. All the authors discussed the results and commented on and proofread the final form of the manuscript.

Conflicts of interest

There are no conflicts to declare.

Acknowledgements

We gratefully acknowledge the support from the National Natural Science Foundation of China (22471094 and 22271116 for M. W.), the fellowship of China Postdoctoral Science Foundation (2023M741338 for H. Y.), and Postdoctoral Fellowship Program of CPSF (GZC20230940 for H. Y.). We thank the staff at BL17B1 beamline of the National Facility for Protein Science in Shanghai (NFPS), Shanghai Advanced Research Institute, CAS, for providing technical support in X-ray diffraction data collection and analysis.

References

1 S. Saha, I. Regeni and G. H. Clever, Structure relationships between bis-monodentate ligands and coordination driven self-assemblies, *Coord. Chem. Rev.*, 2018, **374**, 1–14.
2 E. G. Percástegui, T. K. Ronson and J. R. Nitschke, Design and applications of water-soluble coordination cages, *Chem. Rev.*, 2020, **120**, 13480–13544.

© 2025 The Author(s). Published by the Royal Society of Chemistry

Open Access Article. Published on 07 March 2025. Downloaded on 2/15/2026 10:58:22 PM. This article is licensed under a Creative Commons Attribution-NonCommercial 3.0 Unported Licence.

3 D. Fujita, Y. Ueda, S. Sato, N. Mizuno, T. Kumasaka and M. Fujita, Self-assembly of tetravalent Goldberg polyhedra from 144 small components, *Nature*, 2016, **540**, 563–566.
4 T. Wu, Z. Jiang, Q. Bai, Y. Li, S. Mao, H. Yu, L. Wojtas, Z. Tang, M. Chen, Z. Zhang, T.-Z. Xie, M. Wang, X. Li and P. Wang, Supramolecular triangular orthobicupola: Self-assembly of a giant Johnson solid J_{27}, *Chem*, 2021, **7**, 2429–2441.
5 H. Wang, L.-P. Zhou, Y. Zheng, K. Wang, B. Song, X. Yan, L. Wojtas, X.-Q. Wang, X. Jiang, M. Wang, Q.-F. Sun, B. Xu, H.-B. Yang, A. C. H. Sue, Y.-T. Chan, J. L. Sessler, Y. Jiao, P. J. Stang and X. Li, Double-layered supramolecular prisms self-assembled by geometrically non-equivalent tetratopic subunits, *Angew. Chem., Int. Ed.*, 2021, **60**, 1298–1305.
6 S. Pullen, J. Tessarolo and G. H. Clever, Increasing structural and functional complexity in self-assembled coordination cages, *Chem. Sci.*, 2021, **12**, 7269–7293.
7 J. E. M. Lewis, A. B. S. Elliott, C. J. McAdam, K. C. Gordon and J. D. Crowley, 'Click' to functionalise: synthesis, characterisation and enhancement of the physical properties of a series of exo- and endo-functionalised Pd_2L_4 nanocages, *Chem. Sci.*, 2014, **5**, 1833–1843.
8 Y. Tsujimoto, T. Kojima and S. Hiraoka, Rate-determining step in the self-assembly process of supramolecular coordination capsules, *Chem. Sci.*, 2014, **5**, 4167–4172.
9 Y.-S. Chen, E. Solel, Y.-F. Huang, C.-L. Wang, T.-H. Tu, E. Keinan and Y.-T. Chan, Chemical mimicry of viral capsid self-assembly *via* corannulene-based pentatopic tectons, *Nat. Commun.*, 2019, **10**, 3443.
10 M. Yoshizawa, M. Tamura and M. Fujita, Diels-Alder in Aqueous Molecular Hosts: Unusual Regioselectivity and Efficient Catalysis, *Science*, 2006, **312**, 251–254.
11 R. Banerjee, D. Chakraborty, W.-T. Jhang, Y.-T. Chan and P. S. Mukherjee, Structural switching of a distorted trigonal metal–organic cage to a tetragonal cage and singlet oxygen mediated oxidations, *Angew. Chem., Int. Ed.*, 2023, **62**, e202305338.
12 I. Jahović, Y. Yang, T. K. Ronson and J. R. Nitschke, Capture of singlet oxygen modulates host-guest behavior of coordination cages, *Angew. Chem., Int. Ed.*, 2023, **62**, e202309589.
13 H. Lee, J. Tessarolo, D. Langbehn, A. Baksi, R. Herges and G. H. Clever, Light-powered dissipative assembly of diazocine coordination cages, *J. Am. Chem. Soc.*, 2022, **144**, 3099–3105.
14 L. Catti, H. Narita, Y. Tanaka, H. Sakai, T. Hasobe, N. V. Tkachenko and M. Yoshizawa, Supramolecular singlet fission of pentacene dimers within polyaromatic capsules, *J. Am. Chem. Soc.*, 2021, **143**, 9361–9367.
15 S.-J. Hu, X.-Q. Guo, L.-P. Zhou, D.-N. Yan, P.-M. Cheng, L.-X. Cai, X.-Z. Li and Q.-F. Sun, Guest-driven self-assembly and chiral induction of photofunctional lanthanide tetrahedral cages, *J. Am. Chem. Soc.*, 2022, **144**, 4244–4253.
16 D. Chakraborty, R. Saha, J. K. Clegg and P. S. Mukherjee, Selective separation of planar and non-planar hydrocarbons using an aqueous Pd_6 interlocked cage, *Chem. Sci.*, 2022, **13**, 11764–11771.
17 R. Sumida, Y. Tanaka, K. Niki, Y. Sei, S. Toyota and M. Yoshizawa, Cyclic monoterpenes trapped in a polyaromatic capsule: unusual selectivity, isomerization, and volatility suppression, *Chem. Sci.*, 2021, **12**, 9946–9951.
18 K. Yazaki, M. Akita, S. Prusty, D. K. Chand, T. Kikuchi, H. Sato and M. Yoshizawa, Polyaromatic molecular peanuts, *Nat. Commun.*, 2020, **8**, 15914.
19 S. Ghosal, A. Das, D. Roy and J. Dasgupta, Tuning light-driven oxidation of styrene inside water-soluble nanocages, *Nat. Commun.*, 2024, **15**, 1810.
20 M. Yoshizawa, M. Tamura and M. Fujita, Diels-Alder in aqueous molecular hosts: unusual regioselectivity and efficient catalysis, *Science*, 2006, **312**, 251–254.
21 V. A. Rinshad, M. Aggarwal, J. K. Clegg and P. S. Mukherjee, Harnessing a Pd_4 water-soluble molecular capsule as a size-selective catalyst for targeted oxidation of alkyl aromatics, *JACS Au*, 2024, **4**, 3238–3247.
22 D. Prajapati, J. K. Clegg and P. S. Mukherjee, Formation of a low-symmetry Pd_8 molecular barrel employing a hetero donor tetradentate ligand, and its use in the binding and extraction of C_{70}, *Chem. Sci.*, 2024, **15**, 12502–12510.
23 R.-J. Li, A. Tarzia, V. Posligua, K. E. Jelfs, N. Sanchez, A. Marcus, A. Baksi, G. H. Clever, F. Fadaei-Tirani and K. Severin, Orientational self-sorting in cuboctahedral Pd cages, *Chem. Sci.*, 2022, **13**, 11912–11917.
24 R.-J. Li, A. Marcus, F. Fadaei-Tirani and K. Severin, Orientational self-sorting: formation of structurally defined Pd_4L_8 and Pd_6L_{12} cages from low-symmetry dipyridyl ligands, *Chem. Commun.*, 2021, **57**, 10023–10026.
25 D. Ogata and J. Yuasa, Dynamic open coordination cage from nonsymmetrical imidazole–pyridine ditopic ligands for turn-on/off anion binding, *Angew. Chem., Int. Ed.*, 2019, **58**, 18424–18428.
26 S. S. Mishra, S. V. K. Kompella, S. Krishnaswamy, S. Balasubramanian and D. K. Chand, Low-symmetry self-assembled coordination complexes with exclusive diastereoselectivity: experimental and computational studies, *Inorg. Chem.*, 2020, **59**, 12884–12894.
27 A. Tarzia, J. E. M. Lewis and K. E. Jelfs, High-throughput computational evaluation of low symmetry Pd_2L_4 cages to aid in system design, *Angew. Chem., Int. Ed.*, 2021, **60**, 20879–20887.
28 H. Yu, Z. Guo, N. Han, J. Shi, X. Jiang, Q. Bai, Z. Zhang, P. Wang and M. Wang, Construction of outward-everted metal–organic cages induced by steric hindrance groups based on dissymmetrical ligands, *Cell Rep. Phys. Sci.*, 2023, **4**, 101631.
29 H. Yu, J. Li, C. Shan, T. Lu, X. Jiang, J. Shi, L. Wojtas, H. Zhang and M. Wang, Conformational control of a metallo-supramolecular cage *via* the dissymmetrical modulation of ligands, *Angew. Chem., Int. Ed.*, 2021, **60**, 26523–26527.
30 J. E. M. Lewis, A. Tarzia, A. J. P. White and K. E. Jelfs, Conformational control of Pd_2L_4 assemblies with unsymmetrical ligands, *Chem. Sci.*, 2020, **11**, 677–683.

Open Access Article. Published on 07 March 2025. Downloaded on 2/15/2026 10:58:22 PM. This article is licensed under a Creative Commons Attribution-NonCommercial 3.0 Unported Licence.

31 J. E. M. Lewis, Pseudo-heterolepticity in low-symmetry metal–organic cages, *Angew. Chem., Int. Ed.*, 2022, **61**, e202212392.
32 W. M. Bloch, Y. Abe, J. J. Holstein, C. M. Wandtke, B. Dittrich and G. H. Clever, Geometric complementarity in assembly and guest recognition of a bent heteroleptic *cis*-$[Pd_2L^A{}_2L^B{}_2]$ coordination cage, *J. Am. Chem. Soc.*, 2016, **138**, 13750–13755.
33 W. M. Bloch, J. J. Holstein, W. Hiller and G. H. Clever, Morphological control of heteroleptic *cis*- and *trans*-$Pd_2L_2L'_2$ cages, *Angew. Chem., Int. Ed.*, 2017, **56**, 8285–8289.
34 Y. Liu, S.-H. Liao, W.-T. Dai, Q. Bai, S. Lu, H. Wang, X. Li, Z. Zhang, P. Wang, W. Lu and Q. Zhang, Controlled construction of heteroleptic $[Pd_2(L^A)_2(L^B)(L^C)]^{4+}$ cages: a facile approach for site-selective endo-functionalization of supramolecular cavities, *Angew. Chem., Int. Ed.*, 2023, **62**, e202217215.
35 M. Yamashina, T. Yuki, Y. Sei, M. Akita and M. Yoshizawa, Anisotropic expansion of an M_2L_4 coordination capsule: host capability and frame rearrangement, *Chem.–Eur. J.*, 2015, **21**, 4200–4204.
36 X. Yan, T. R. Cook, P. Wang, F. Huang and P. J. Stang, Highly emissive platinum(II) metallacages, *Nat. Chem.*, 2015, **7**, 342–348.
37 R.-J. Li, F. Fadaei-Tirani, R. Scopelliti and K. Severin, Tuning the size and geometry of heteroleptic coordination cages by varying the ligand bent angle, *Chem.–Eur. J.*, 2021, **27**, 9439–9445.
38 S. Sudan, R.-J. Li, S. M. Jansze, A. Platzek, R. Rudolf, G. H. Clever, F. Fadaei-Tirani, R. Scopelliti and K. Severin, Identification of a heteroleptic $Pd_6L_6L'_6$ coordination cage by screening of a virtual combinatorial library, *J. Am. Chem. Soc.*, 2021, **143**, 1773–1778.
39 T. Abe, N. Sanada, K. Takeuchi, A. Okazawa and S. Hiraoka, Assembly of six types of heteroleptic Pd_2L_4 cages under kinetic control, *J. Am. Chem. Soc.*, 2023, **145**, 28061–28074.
40 K. Wu, E. Benchimol, A. Baksi and G. H. Clever, Non-statistical assembly of multicomponent $[Pd_2ABCD]$ cages, *Nat. Chem.*, 2024, **16**, 584–591.
41 P. Molinska, A. Tarzia, L. Male, K. E. Jelfs and J. E. M. Lewis, Diastereoselective self-assembly of low-symmetry Pd_nL_{2n} nanocages through coordination-sphere engineering, *Angew. Chem., Int. Ed.*, 2023, **62**, e202315451.
42 D. Preston and J. D. Evans, A lantern-shaped Pd(II) cage constructed from four different low-symmetry ligands with positional and orientational control: an ancillary pairings approach, *Angew. Chem., Int. Ed.*, 2023, **62**, e202314378.
43 M. Parbin, V. Sivalingam and D. K. Chand, Highly anisotropic $Pd_2L_2L_2$ and $Pd_2L_2L_2$ type cages by heteromeric completive self-sorting, *Angew. Chem., Int. Ed.*, 2024, **63**, e202410219.
44 A. P. Birvé, H. D. Patel, J. R. Price, W. M. Bloch and T. Fallon, Guest-dependent isomer convergence of a permanently fluxional coordination cage, *Angew. Chem., Int. Ed.*, 2022, **61**, e202115468.
45 M. R. Black, S. Bhattacharyya, S. P. Argent and B. S. Pilgrim, Structural transformations of metal–organic cages through tetrazine-alkene reactivity, *J. Am. Chem. Soc.*, 2024, **146**, 28233–28241.
46 S. Samantray, S. Krishnaswamy and D. K. Chand, Self-assembled conjoined-cages, *Nat. Commun.*, 2020, **11**, 880.
47 Q.-F. Sun, S. Sato and M. Fujita, An $M_{12}(L^1)_{12}(L^2)_{12}$ cantellated tetrahedron: a case study on mixed-ligand self-assembly, *Angew. Chem., Int. Ed.*, 2014, **53**, 13510–13513.
48 D. K. Chand, K. Biradha, M. Kawano, S. Sakamoto, K. Yamaguchi and M. Fujita, Dynamic self-assembly of an M_3L_6 molecular triangle and an M_4L_8 tetrahedron from naked PdII ions and bis(3-pyridyl)-substituted arenes, *Chem.–Asian J.*, 2006, **1**, 82–90.
49 R. Zhu, W. M. Bloch, J. J. Holstein, S. Mandal, L. V. Schäfer and G. H. Clever, Donor-site-directed rational assembly of heteroleptic *cis*-$[Pd_2L_2L'_2]$ coordination cages from picolyl ligands, *Chem.–Eur. J.*, 2018, **24**, 12976–12982.
50 R. A. S. Vasdev, D. Preston, C. A. Casey-Stevens, V. Martí-Centelles, P. J. Lusby, A. L. Garden and J. D. Crowley, Exploiting supramolecular interactions to control isomer distributions in reduced-symmetry $[Pd_2L_4]^{4+}$ cages, *Inorg. Chem.*, 2023, **62**, 1833–1844.
51 B. Chen, J. J. Holstein, A. Platzek, L. Schneider, K. Wu and G. H. Clever, Cooperativity of steric bulk and H-bonding in coordination sphere engineering: heteroleptic Pd^{II} cages and bowls by design, *Chem. Sci.*, 2022, **13**, 1829–1834.

© 2025 The Author(s). Published by the Royal Society of Chemistry